

Influence of finite bandwidth on the propagation of information in fast- and slow-light media

Heisuke Amano and Makoto Tomita

Department of Physics, Faculty of Science, Shizuoka University, 836, Ohya, Suruga-ku, Shizuoka, 422-8529, Japan

(Received 8 March 2016; published 28 June 2016)

We examined the propagation of information encoded as nonanalytical points on temporally Gaussian-shaped optical pulses in fast- and slow-light systems. The bandwidth of the input pulses determined the sharpness of the nonanalytical points. A sharp bending nonanalytical point propagated with luminal velocity in both fast- and slow-light systems, in good agreement with relativistic causality. As the bandwidth was reduced, the bending point became broad and propagated with the relevant group velocities. This transition was, however, qualitatively different in the fast- and slow-light systems. We also examined the predictability of the future pulse shape beyond the practical nonanalytical point on the basis of the expansion. When the bandwidth was reduced below a critical value, the expansion well predicted the future pulse shape.

DOI: [10.1103/PhysRevA.93.063854](https://doi.org/10.1103/PhysRevA.93.063854)**I. INTRODUCTION**

Superluminal propagation of optical pulses has been observed in many systems, including, atomic absorption and gain lines [1–4], microcavities [5,6], metamaterials [7,8], and photonic structures [9–11], through the control of quantum coherence or manipulation of the photonic structures. Superluminal pulse propagation is a ubiquitous effect appearing in any dispersive system [12]. Although this velocity is seemingly paradoxical in the context of Einstein's special relativity, it is now well understood that the arrival of the smooth superluminal pulse peak does not contain true information, because the arrival of the peak can be predicted on the basis of the expansion of the early part of the pulse [13–16]. It was demonstrated experimentally that a Gaussian-shaped peak exited from the far side of a negative-group-velocity medium, even though the incident pulse was terminated before its Gaussian peak [17].

There have been long debates surrounding the information velocity in superluminal media. Historically, Sommerfeld and Brillouin showed that, although the main signal propagates through the medium with a group velocity, the front edge propagates at c , the velocity of light in a vacuum [18–20]. They claimed that the true signal was carried by the front; thus, the superluminal pulse propagation of the pulse peak is not contradictory to Einstein's special relativity. The idea was developed that true information was encoded on nonanalytical points along the wave packets [21–24]. The front edges can be considered as nonanalytical points.

The idea that the true information is included on the nonanalytical points and that the propagation velocity of the information is equal to that of the nonanalytical points seems to be fundamentally reasonable and has been accepted by many researchers. Strictly, however, ideal nonanalytical points, as well as ideal analytical functions, are mathematical illusions. Practically, there are many questions to be discussed because there are crucial gaps between the ideal nonanalytical points and practical nonanalytical points. For example, mathematically, a Gaussian pulse has tails extending infinitely far back and forth in time. Actually, there should be a front and an end; i.e., a nonanalytical point, in any pulse, in accordance with the discussions by Sommerfeld and Brillouin. In addition, it is unclear whether such a front is truly localized at an

infinitesimal time point. Second, mathematically, an analytical function is differentiable at any order; therefore, any tiniest leading edge of a smooth Gaussian pulse determines the entire pulse. Practically, it is obvious that the leading edge must have sufficient photons. The question then arises as to how many photons are necessary to reconstruct the forthcoming pulse shape. Third, real experimental data suffer fluctuations and noise; thus, it is always difficult to determine the exact time point of the nonanalytical point [22,23,25–28]. Finally, if the information velocity is defined on the basis of the nonanalytical points, then the signal velocity should always be the same as the speed of light in a vacuum, raising the question as to whether there are any practical uses of slow and fast light [28].

The fluctuations and noise represent one of the most intensively studied effects [22,23,25–28]. Stenner *et al.* examined the velocity of detectable information experimentally in superluminal-group-velocity media, defining the location of the nonanalytical point on the basis of the bit error rate [22,23]. To achieve a given signal-to-noise ratio at the output of an amplifying medium, a larger signal was required, resulting in retardation of the signal. They concluded that the time to detect information propagating through a fast-light medium was longer than the time required to detect the same information traveling through a vacuum. Dorrah and Mojahedi investigated the effects of the propagation distance [27]. They showed that the relative strength of the detector noise with respect to the medium noise critically affected the signal velocity. From the point of view of the question on realistic uses of slow and fast light, Yang introduced another definition of information velocity, defining the velocity as the ratio of the propagation distance to the minimum time required to complete the part of the pulse that carried the information of interest [28].

Our interest here is in another aspect of the nonanalytical points: that is, the predictability of the future pulse shape beyond the practical nonanalytical point. An ideal nonanalytical point localizes at an infinitesimal time point; thus, it requires infinite spectral bandwidth and infinite energy. It is impossible to realize an ideal nonanalytical point in the laboratory. In contrast, the bandwidth of any practical nonanalytical point is restricted to a finite value; therefore, the nonanalytical point acquires analyticity and delocalizes, spreading into a certain time region. This suggests that the practical nonanalytical point

neither disconnects completely nor connects completely to the previous and following regions in the pulse.

In this paper, we examine the propagation of the practical nonanalytical points that are relevant to a finite bandwidth. We first examined experimentally the propagation of a bending nonanalytical point encoded on a temporally Gaussian-shaped optical pulse in fast- and slow-light systems using optical ring resonators. We controlled the sharpness of the bending point. When the bandwidth was sufficiently large, the bending point acted as a nonanalytical point and propagated with the velocity of light in a vacuum or in the background medium, independent of the group velocity. This is in agreement with relativistic causality. As the sharpness of the bending points was reduced, the point was advanced and delayed in the fast- and slow-light systems, respectively. This transition was, however, qualitatively different in the fast- and slow-light systems. From the point of view of relativistic causality, the fast propagation of the practical nonanalytical point in the fast-light medium suggests that the expansion of the early part of the pulse can predict the forthcoming bending point. Therefore, we also examined the predictability of the forthcoming pulse shape beyond the practical nonanalytical point on the basis of the expansion.

II. EXPERIMENTS

Our experimental setup was similar to previous experiments [29], and is illustrated schematically in Fig. 1(a). We used fiber ring resonators, which offer highly controllable dispersion via the cavity loss x and coupling strength between the fiber and the ring resonator, y . Note that our interest here lies in the propagation of the practical nonanalytical points and not in the dispersion characteristics of the ring resonators, which have already been studied in detail [5,6]. The stationary input-output characteristics of the resonator can be analyzed on the basis of directional coupling theory. The transmitted light intensity $T(\nu)$, as a function of incident laser frequency ν , shows a periodic dip structure due to resonance. The dispersion relationship depends on the loss and coupling strength. For the undercoupling condition ($x < y$), the transmission phase $\theta(\omega)$ shows an anomalous dispersion at the center of the resonance.

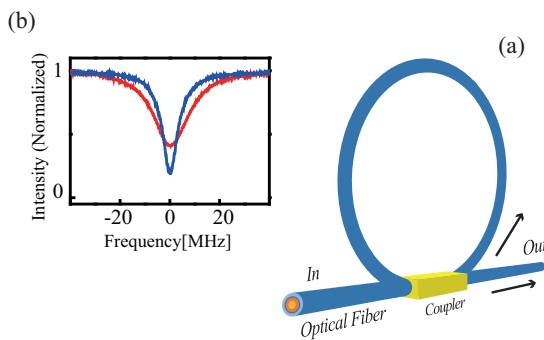


FIG. 1. (a) Schematic illustration of the experimental setup. (b) Experimental observations of the resonance spectra of the ring resonators. The blue and red lines represent the undercoupling and overcoupling conditions, respectively. The resonance widths were 7.6 MHz and 11.4 MHz, respectively.

The group delay is expected to be negative, $\tau_g = \partial\theta/\partial\omega < 0$, corresponding to superluminal pulse propagation, i.e., fast light. In contrast, for the overcoupling condition ($x > y$), the transmission phase shows normal dispersion, and one would expect slow light.

In the current study, 90:10 and 80:20 couplers were used to achieve undercoupling and overcoupling conditions, respectively. We inserted additional loss elements within the ring resonator to control the loss parameter. The physical length of the ring was $L_R = 100$ cm. Figure 1(b) shows an example of a transmission spectrum as a function of detuning frequency; the blue and red lines represent the resonance spectra of the ring resonator for the under-coupling and over-coupling conditions, respectively. The resonance widths are $\delta\nu_R = 7.6$ MHz and 11.4 MHz, respectively. An Er-fiber laser was used as the incident light source. The spectral width was 1 kHz, and the laser frequency was tuned by piezoelectric control of the cavity length. We prepared Gaussian-shaped pulses, which were encoded with bending nonanalytical points at time t_{NA} on the leading side of the pulse:

$$E_{in}(t, \infty) = \begin{cases} \alpha t + \beta, & t \leq t_{NA}, \\ \exp[-(\frac{t}{t_p})^2], & t_{NA} < t, \end{cases} \quad (1)$$

where $t_p = 180$ ns, $t_{NA} = -120$ ns, $\alpha = 1.2 \times 10^{-3}$ ns $^{-1}$, and $\beta = 0.79$. In contrast to traditional nonanalytical points, the function of Eq. (1) is continuous at t_{NA} , but the first-order derivative is discontinuous, $\lim_{\epsilon \rightarrow 0} \partial E_{in}(t)/\partial t|_{t_{NA}-\epsilon} \neq \lim_{\epsilon \rightarrow 0} \partial E_{in}(t)/\partial t|_{t_{NA}+\epsilon}$; thus, t_{NA} is a bending nonanalytical point. The notation “ ∞ ” in $E_{in}(t, \infty)$ indicates that the point at t_{NA} has initially infinite bandwidth. The Fourier spectrum $E_{in}(\nu, \infty)$ of Eq. (1) has long wings in the higher- and lower-frequency regions, which are responsible for the bending point. These components are small in intensity, but critically important for the sharpness of the bending point. We controlled the sharpness of the bend using a bandpass filter. The Fourier spectrum of the original pulse was passed through a filter function $F(\nu, \delta\nu_B)$, where $\delta\nu_B$ is the bandwidth. This function was then inversely Fourier transformed. We refer to this filtered input pulse as $E_{fil}(t, \delta\nu_B)$. A series of optical pulses of different sharpness at the bending point was generated from the laser using a LiNbO₃ (LN) modulator. The repetition rate was 100 kHz and the incident power was 0.1 mW. Transmission intensity through the system was observed using an InGaAs photodetector and was reordered using a 600-MHz digital oscilloscope.

III. RESULTS

Figure 2 shows the experimental results for the propagation of the bending point through the fast- and slow-light systems. Figure 3 shows an expansion of Fig. 2 around the bending point. In the undercoupled ring resonator, i.e., the fast-light system [Figs. 2(a1) and 3(a)], the peak of the Gaussian pulse was not significantly influenced by the presence of the nonanalytical point, and the peak was advanced by -35 ns, similar to the result with the advancement of the original Gaussian pulse without the bending point (not shown). In contrast, the nonanalytical points were neither advanced nor delayed but, rather, appeared as the light entered the ring

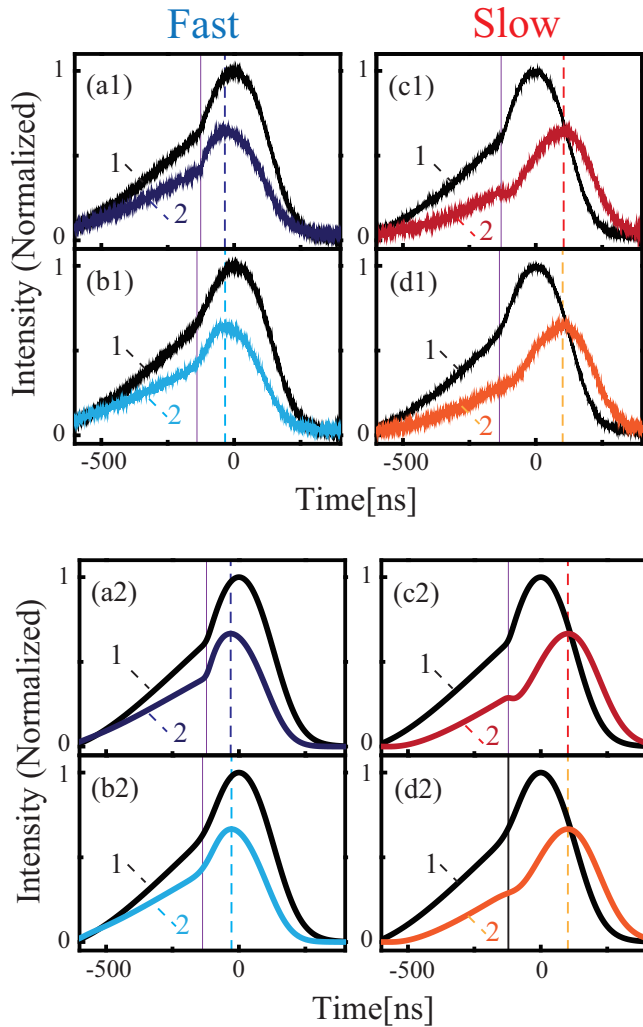


FIG. 2. Propagation of the bending nonanalytical point encoded on Gaussian-shaped pulses at time $t_{NA} = 120$ ns through the ring resonators: (a1)–(d1) experimental observations and (a2)–(d2) numerical simulations. The black (denoted as 1) and colored (denoted as 2) lines in each figure represent input and output pulses, respectively. The left column [(a1), (b1), (a2), and (b2)] and the right column [(c1), (d1), (c2), and (d2)] show the results for undercoupling (fast-light) and overcoupling (slow-light) conditions, respectively. Top [(a1), (c1), (a2), and (c2)] and bottom [(b1), (d1), (b2), and (d2)] show the results without and with the bandpass filter of $\delta\nu_B = 12$ MHz, respectively. The dotted colored vertical lines represent the time of the peak in the output pulses. The Gaussian pulse peak shows negative [-35 ns in (b1)] and positive [102 ns in (d1)] delays for the undercoupling and overcoupling conditions, respectively. The solid purple vertical lines represent the time of the bending point in the input pulses. The parameters used in the simulations were $x = 0.9$, $y^2 = 0.92$, and $y^2 = 0.84$ for the undercoupling and overcoupling conditions, respectively.

resonator within the experimental resolution (2 ns). The experimental result suggests, therefore, that the nonanalytical point propagated with the light velocity in the background medium, independently of the group velocity. Here, we refer to this velocity as a luminal velocity. In traditional experiments [22–24], the front edge or discontinuous points in the pulse

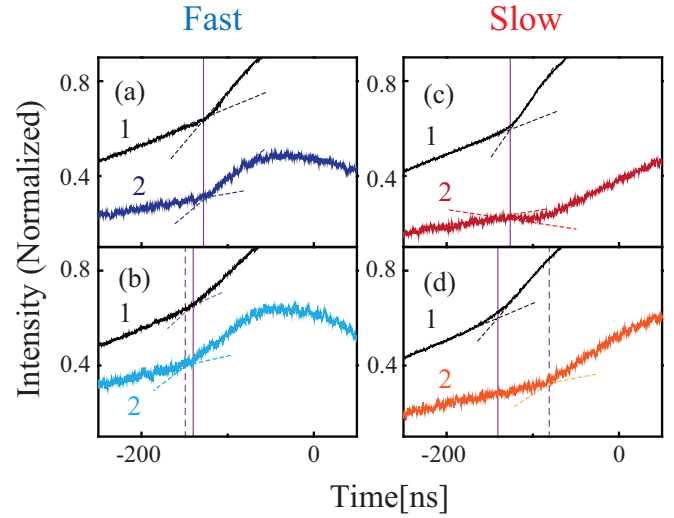


FIG. 3. Expansion of Fig. 2 around the bending point; (a)–(d) correspond to Figs. 2(a1)–2(d1), respectively. The solid and dotted purple vertical lines represent the time of the bending point in the input and output pulses, respectively. In (a) and (c), the two vertical lines (i.e., solid and dotted lines) are overlapped with respect to each other. The sharp bending points propagated with luminal velocity in both (a) fast- and (b) slow-light systems. The broad bending point showed (c) negative (-10 ns) and (d) positive (56 ns) delays.

envelope were examined as nonanalytical points. A time point at which any order of the derivatives is discontinuous could also be recognized as a nonanalytical point [30]. The experimental results shown in Figs. 2(a1) and 3(a) were, thus, in good agreement with arguments relevant to relativistic causality that the sharp bending point propagates with luminal velocity. Figures 2(b1) and 3(b) show the propagation of the bending nonanalytical point, in which the sharpness of the bend was reduced using a bandpass filter of $\delta\nu_B = 12$ MHz. As a result of the bandwidth restriction, the bending point became broad and advanced by -10 ns. Figures 2(c1) and 2(d1) and Figs. 3(c) and 3(d) show similar experimental results in the overcoupled ring resonator, i.e., the slow-light system. The Gaussian pulse peak was delayed by 102 ns, the same as the delay of the Gaussian pulse without the bending point (not shown). The sharp bending point propagated with luminal velocity [Figs. 2(c1) and 3(c)], as was the case in the fast-light system. The characteristic features in the transmitted pulse profile were, however, different between the fast- and slow-light systems. In the fast-light system [Figs. 2(a1) and 3(a)], the bending point was followed by the Gaussian peak immediately after the bending point. In contrast, in the slow-light system [Figs. 2(c1) and 3(c)], a dip and plateau appeared just after the point. This is reasonable because the peak moved in negative and positive time directions in the fast- and slow-light systems, respectively, while the nonanalytical point stayed at the original time point in both systems; thus, the interval between the Gaussian peak and the bending point became narrow in the fast-light system and wide in the slow-light system. This effect resulted in the gap and the plateau only in the slow-light system. To analyze the details, we systematically examined the propagation of the bending

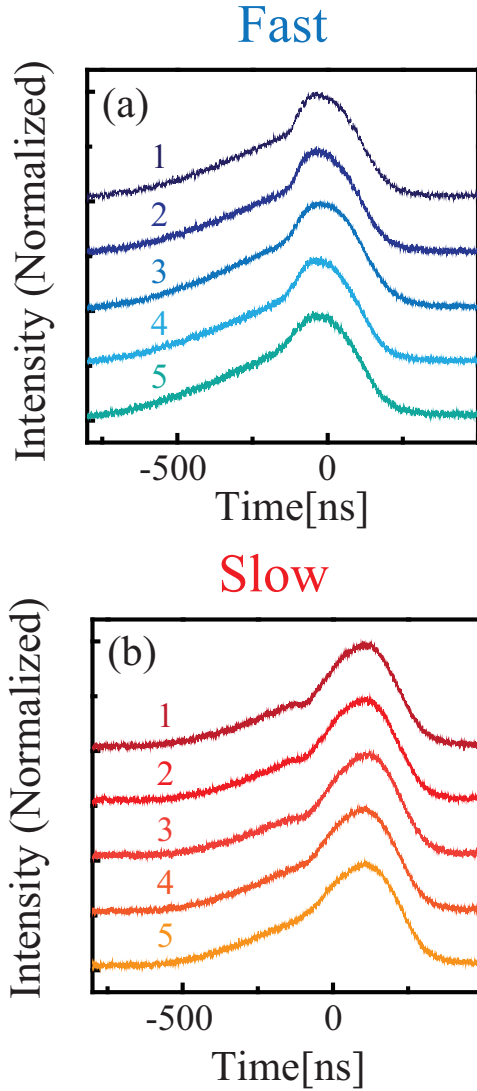


FIG. 4. Propagation of the bending point encoded on Gaussian-shaped pulses for different values of the bandwidth $\delta\nu_B$. Experimental results for (a) undercoupling (fast-light) and (b) overcoupling (slow-light) conditions, respectively. In both (a) and (b), from top to bottom, the bandwidth was 40, 24, 16, 12, and 8 MHz.

point for different values of $\delta\nu_B$. Figures 4(a) and 4(b) show the experimental results of the transmitted pulse profile in the fast- and slow-light systems, respectively. In Fig. 5, the early edges of the bending region in the transmitted pulses are plotted as a function of $\delta\nu_B$ for both the fast- and slow-light systems. In the fast-light system, the sharp bending gradually became smooth and the advancement increased monotonically as the bandwidth was reduced. In contrast, in the slow-light system, the dip was gradually filled as the bandwidth was reduced; the delay time jumped towards the relevant group delay when the dip was completely filled. In Fig. 5, in the slow-light case, the error bars were large for bandwidths below 20 MHz as the gap and plateau made it difficult to determine accurately the transition region.

In Figs. 2(a2)–2(d2) and Fig. 6, numerical simulations are shown for the transmitted pulse profile. The simulations well

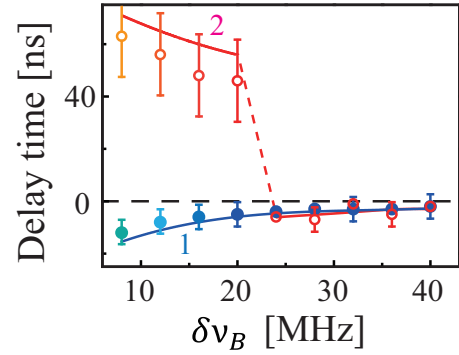


FIG. 5. Delay time of the early edge of the bending point in the output pulses as a function of the bandwidth $\delta\nu_B$. The solid (blue series) and open (red series) circles are experimental results for the under- and overcoupling conditions, respectively. The colors of circles correspond to those used in Fig. 4. The solid blue (denoted as 1) and red (denoted as 2) lines are calculations for the under- and overcoupling conditions, respectively.

captured the main features of the experiments. In particular, for the slow-light system, the sharp bending point was followed by a dip and plateau [Fig. 6(a3)]. The dip was gradually filled [Figs. 6(b3) and 6(c3)] as the bandwidth was reduced, and the delay time jumped towards the group delay when the dip was totally filled [Fig. 6(d3)]. For a bandwidth below 24 MHz,

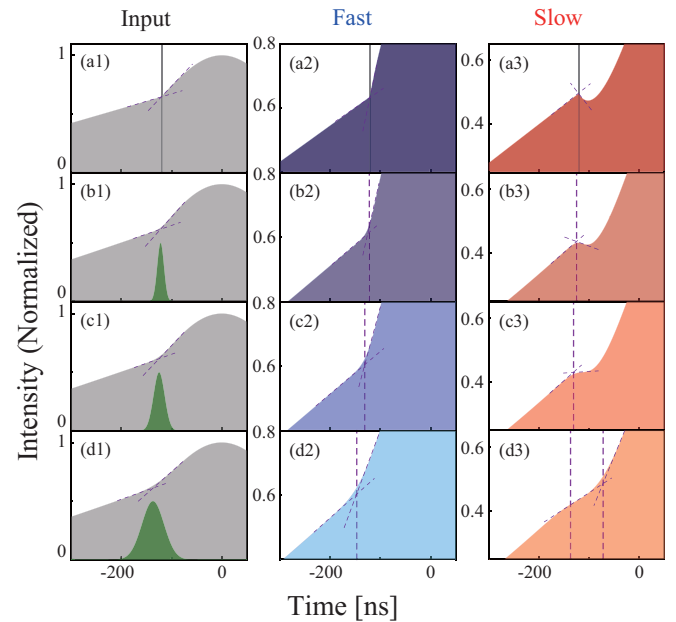


FIG. 6. Numerical simulations for the propagation of the practical bending nonanalytical point encoded on Gaussian-shaped pulses at time $t_{NA} = -120$ ns. The left column [(a1)–(d1)] shows input pulses. The green hatched shapes represent the filter function. The middle [(a2)–(d2)] and right [(a3)–(d3)] columns are the output pulses through the undercoupling (fast-light) and overcoupling (slow-light) conditions, respectively. The bandwidth was, from top to bottom, infinite, 40, 24, and 12 MHz, respectively. The solid and dotted purple lines represent the times of the bending point in the input and output pulses, respectively. For the slow-light system, a dip and plateau appeared just after the bending point [(a3), (b3), and (c3)].

the advancement and delay approached those of the Gaussian pulse peak, and the entire pulse shapes were totally advanced or delayed, keeping the shape unchanged. The broad bending point cannot transfer information; thus, it is not contradictory to relativity.

We add three notes. First, for the input pulses represented by Eq. (1), the bending point was encoded in the leading section of the pulse; i.e., before the peak ($t_{NA} < 0$). When the bending point was encoded on the trailing section of the pulse after the peak ($0 < t_{NA}$), we obtained the opposite results with respect to the fast- and slow-light systems. That is, in the fast-light system, a dip and plateau appeared just before the bending point. In the slow-light system, the dip did not appear. These opposite results observed under the condition $0 < t_{NA}$ are also reasonable because the nonanalytical point stayed at the original time point; thus, the interval between the Gaussian peak and the bending point became wide in the fast-light system, while this interval became narrow in the slow-light system. Similar results were confirmed in Lorentz-type absorbing and amplifying resonance lines (i.e., fast- and slow-light media, respectively).

Second, in our experiments, the peak of the Gaussian pulse was not seriously influenced by the presence of the nonanalytical point (Fig. 2). Recently, Yang [28] introduced a new definition of information velocity, as the ratio of the propagation distance to the minimum time required to complete any given information transfer process. In the context of this discussion, for the preservation of the Gaussian pulse peak in Fig. 2, a longer time interval between the nonanalytical point and the pulse peak was necessary than the minimum time specified above.

Finally, in previous experiments [29], the functional form for the slowly varying envelope of the input pulses, $f(t) = A \exp[-|t/t_p|^\alpha]$ was used, where the parameter α controlled the sharpness of the pulse peak. For $\alpha = 1$, the pulse is exponential on both sides. In this case, the pulse peak is mathematically a nonanalytical point. For $\alpha = 2$, the pulse is the traditional Gaussian pulse, where the pulse peak becomes smooth and mathematically analytical. The present method, based on bandwidth restriction, is a more general approach to examining the effect of sharpness of the practical nonanalytical points and is applicable to any type of nonanalytical point.

IV. DISCUSSION: PREDICTABILITY

In our experiments, the sharp bending point propagated with luminal velocity in both fast- and slow-light media, consistent with relativistic causality [13–24]. As the bandwidth was reduced, the bending point became broad and propagated with the relevant group velocities. For the case of a traditional Gaussian pulse peak, it has been debated whether the arrival of the smooth pulse peak can be predicted on the basis of the expansion of the leading part of the pulse, thus meaning that the pulse peak does not contain true information [21]. We developed this idea to incorporate a bandwidth-restricted practical nonanalytical point. From the point of view of relativistic causality, the fast propagation of the practical nonanalytical point in the fast-light medium suggests that the expansion around an earlier time point

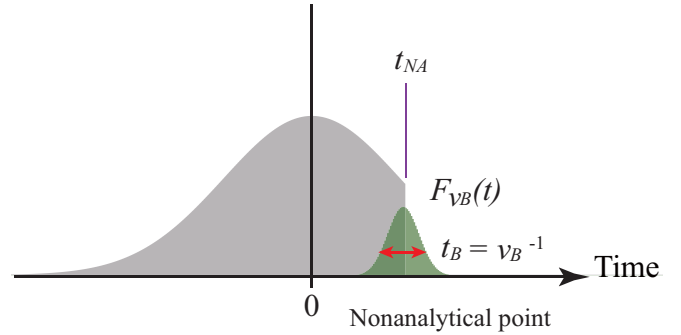


FIG. 7. Illustration, shown as a gray hatched shape, of Gaussian-shaped pulses encoded with discontinuous nonanalytical points at time t_{NA} on the trailing side of the pulse. The pulse shape is represented by Eq. (2). The green hatched shape represents the filter function.

$t_0 < t_{NA}$ can predict the forthcoming pulse shape. For the confirmation of this predictability of the function form, we consider a Taylor expansion for the following pulse shape:

$$E_{in}(t, \infty) = \begin{cases} \exp[-(\frac{t}{t_p})^2], & t \leq t_{NA}, \\ 0, & t_{NA} < t, \end{cases} \quad (2)$$

where $t_p = 180$ ns and $t_{NA} = -120$ ns. The function form is illustrated schematically in Fig. 7. Here, we discuss the discontinuous nonanalytical point $\lim_{\varepsilon \rightarrow 0} E_{in}(t_{NA} - \varepsilon) \neq \lim_{\varepsilon \rightarrow 0} E_{in}(t_{NA} + \varepsilon)$, rather than the bending nonanalytical point, to more clearly see the effect. For the restriction of the bandwidth, we used a similar process to that used in our experiments. The resulting filtered pulse $E_{fil}(t, \delta v_B)$, was alternatively represented by a convolution of the input pulse, $E_{in}(t, \infty)$, and a Fourier transform of the filter function, $F(t, \delta v_B)$, by Parseval's theorem:

$$E_{fil}(t, \delta v_B) = \int_{-\infty}^{\infty} E_{in}(t') F(t - t', \delta v_B) dt'. \quad (3)$$

Strictly, when the bandwidth is restricted to a finite value, the discontinuous point at t_{NA} is no longer a nonanalytical point in the mathematical sense. However, we consider the point at t_{NA} to represent a rather practical nonanalytical point in physics. As a result of the bandwidth restriction, this point acquired analyticity. We are interested in the predictability of the forthcoming pulse shape beyond t_{NA} . Figure 8 illustrates the Taylor expansion of $E_{in}(t, \infty)$ [without bandwidth reduction; Fig. 8(a)] and $E_{fil}(t, \delta v_B)$ [with the reduction; Figs. 8(b)–8(f)] around $t_0 < 0$. We denote this expansion as

$$\mathcal{T}[E_{fil}(t, \delta v_B); t_0] = \sum_{n=0}^{n_{max}} \frac{1}{n!} a_n(\delta v_B) [t - t_0]^n. \quad (4)$$

Because we developed the expansion over an unusually high order range, we paid special attention to the numerical errors. The significant figure was enhanced up to 150; we confirmed that a significant figure of 300 also gave the same results. The red and light blue lines in Fig. 8(a) show $E_{in}(t, \infty)$ and its Taylor expansion $\mathcal{T}[E_{in}(t, \infty); t_0]$, respectively. In

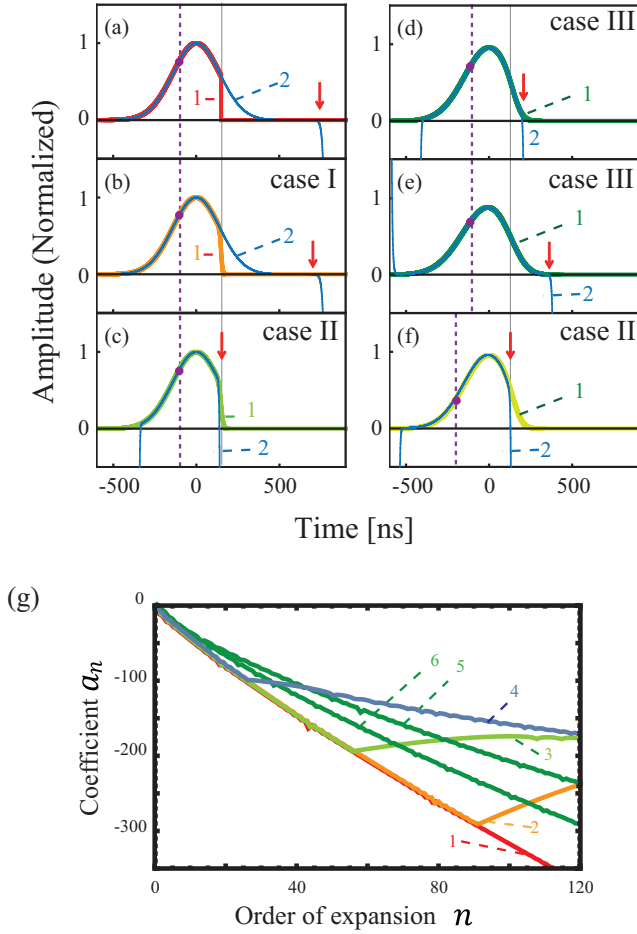


FIG. 8. (a)–(f) Filtered pulses and their expansions. (a) The red line is the original pulse without a bandwidth restriction, $E_{\text{in}}(t, \infty)$. (b) Orange, (c, f) light green, and (d, e) deep green lines (denoted as 1) are bandwidth-restricted pulses, in which the bandwidth was (b) 50, (c) 33, (d) 8.3, and (e) 5.0 MHz. The light blue lines (denoted as 2 in all figures) show the Taylor expansion around $t_0 = -120$ ns. (f) Similar calculations in which the bandwidth was the same as that in (d), but t_0 was shifted to an earlier time $t_0 = -200$ ns. The dotted purple vertical lines indicate the time t_0 . The red arrows represent the time of the radius of convergence. In (a)–(e), the input pulses and expansions overlap in most time regions around the Gaussian peak. (g) The expansion coefficient $a_n(\delta\nu_B)$ as a function of expansion order n for different bandwidths. The filter bandwidth was (1) infinite, (2) 50, (3) 33, (4) 20, (5) 8.3, and (6) 5.0 MHz.

Fig. 8(a), the expansion perfectly predicted the Gaussian-shaped pulses beyond time t_{NA} . This is reasonable because the input pulse at t_0 had no information on the existence of the forthcoming nonanalytical points at t_{NA} ; hence, the expansion perfectly predicted the forthcoming Gaussian pulse shape as an analytical connection of the input pulse at t_0 .

Figures 8(b)–8(e) show a similar expansion for the pulses, $E_{\text{fil}}(t, \delta\nu_B)$, for different values of $\delta\nu_B$. We classify the expansion into three cases, cases I, II, and III depending on the bandwidth $\delta\nu_B$. In case I, we first consider a condition in which the bandwidth is especially broad. Figure 8(b) corresponds to this case, for a bandwidth $\delta\nu_B = 50$ MHz. In this case, the expansion $\mathcal{T}[E_{\text{fil}}(t, \delta\nu_B); t_0]$ predicted the forthcoming

Gaussian peak and the pulse shape beyond t_{NA} , as was the case with the original pulse [Fig. 8(a)]. As the bandwidth was very broad, the nonanalytical point was localized well at t_{NA} and did not affect the expansion around t_0 .

In case II [Fig. 8(c)], the bandwidth of the filter is moderate, $\delta\nu_B = 33$ MHz. The expansion $\mathcal{T}[E_{\text{fil}}(t, \delta\nu_B); t_0]$ well predicted the filtered function $E_{\text{fil}}(t, \delta\nu_B)$ in the time region $t < t_{\text{NA}}$, including the arrival of the Gaussian pulse peak. The expansion, however, became unstable at $t \sim t_{\text{NA}}$ and diverged. It could not predict the forthcoming function shape in the time region after t_{NA} . As the bandwidth was reduced, the nonanalytical point delocalized and emerged in the neighboring time regions. When the earlier boundary of the delocalized nonanalytical region reached t_0 , the anomaly at t_{NA} influenced the expansion around t_0 and the expansion became unstable. The time point t_{NA} disconnected the previous and following time regions of the pulse.

For case III, the bandwidth of the filter is narrow. Figures 8(d) and 8(e) correspond to this case, in which the bandwidth was $\delta\nu_B = 8.3$ and 5.0 MHz, respectively. The expansion $\mathcal{T}[E_{\text{fil}}(t, \delta\nu_B); t_0]$ developed well beyond t_{NA} , correctly predicting the filtered pulse shape $E_{\text{fil}}(t, \delta\nu_B)$. The earlier boundary of the delocalized nonanalytical points spread into early time, before t_0 ; hence, t_0 was totally included in the delocalized nonanalytical region. The input pulse at t_0 had, then, sufficient information to predict the forthcoming filtered pulse shape after t_{NA} . Figure 8(f) shows a similar calculation in which the bandwidth was the same as that shown in Fig. 8(d) (8.3 MHz); however, t_0 had shifted to an earlier time $t_0 = -200$ ns. In this case, the earlier boundary of the delocalized nonanalytical region still did not include t_0 ; thus, the expansion could not predict the function shape after t_{NA} (i.e., belongs to case II).

The distinction among cases I, II, and III also appeared in the development of the expansion coefficient $a_n(\delta\nu_B)$ in Eq. (4). Figure 8(g) shows the expansion coefficients as a function of expansion order n for different bandwidths. The red line in Fig. 8(g) (line 1) shows the expansion coefficient $a_n(\infty)$ for $E_{\text{in}}(t, \infty)$. When the bandwidth was broad, the expansion coefficient $a_n(\delta\nu_B)$ did not differ much from $a_n(\infty)$ [Fig. 8(g), line 2]. This situation corresponds to case I. When the bandwidth was reduced, the expansion coefficient $a_n(\delta\nu_B)$ departed from the curve of $a_n(\infty)$ (line 1) at certain values of n [Fig. 8(g), lines 3 and 4]. We denote this n as the critical expansion order $n_{\text{cri}}(\delta\nu_B)$. It can be seen that $n_{\text{cri}}(\delta\nu_B)$ decreased as the bandwidth was reduced. This situation corresponds to case II. As the bandwidth was reduced further, the expansion coefficient $a_n(\delta\nu_B)$ showed no bend as a function of expansion order n , but developed with a new and different decay rate from that of $a_n(\infty)$ [Fig. 8(g), lines 5 and 6] [i.e., $n_{\text{cri}}(\delta\nu_B)$ did not appear]. This situation corresponds to case III. The expansion around t_0 developed beyond t_{NA} , correctly predicting the filtered Gaussian shape after t_{NA} .

For a quantitative understanding of the characteristic features of cases I, II, and III above, we used a simplified model:

$$\tilde{E}_{\text{in}}(t) = \begin{cases} E_{\text{in}}(t, \infty), & t \leq t_{\text{NA}} - \varepsilon, \\ E_{\text{in}}(t_{\text{NA}}, \infty), & t_{\text{NA}} - \varepsilon < t \leq t_{\text{NA}}, \\ 0, & t_{\text{NA}} < t, \end{cases} \quad (5)$$

where ε is the time duration of the order δv_B^{-1} . Using Eqs. (3) and (5), $\tilde{E}_{\text{fil}}(t, \delta v_B)$ can be written as

$$\begin{aligned}\tilde{E}_{\text{fil}}(t, \delta v_B) &= \int_{-\infty}^{\infty} \tilde{E}_{\text{in}}(t') F(t - t', \delta v_B) dt' \\ &= \int_{-\infty}^{t_{\text{NA}} - \varepsilon} E_{\text{in}}(t', \infty) \delta(t - t') dt' \\ &\quad + E_{\text{in}}(t_{\text{NA}}, \infty) \int_{t_{\text{NA}} - \varepsilon}^{t_{\text{NA}}} F(t - t', \delta v_B) dt' \\ &= E_{\text{in}}(t, \infty) + \varepsilon E_{\text{in}}(t_{\text{NA}}, \infty) F(t - t_{\text{NA}}, \delta v_B).\end{aligned}\quad (6)$$

Here $F(t - t', \delta v_B)$ in Eq. (6) was approximated by $\delta(t - t')$. As an example, when we used a Gaussian-shaped filter function, i.e., $F(\nu) = \exp[-(\nu/\delta v_B)^2]$, then

$$\varepsilon E_{\text{in}}(t_{\text{NA}}, \infty) F(t - t_{\text{NA}}, \delta v_B) \approx E_{\text{in}}(t_{\text{NA}}, \infty) \exp[-(\pi \delta v_B t)^2].\quad (7)$$

We denote the first and second terms in the last equation in Eq. (6) as analytical and nonanalytical terms, respectively. We now presume the value of $\tilde{E}_{\text{fil}}(t_{\text{NA}}, \delta v_B)$, on the basis of the expansion around t_0 , to be

$$\begin{aligned}\mathcal{T}[\tilde{E}_{\text{fil}}(t, \delta v_B); t_0]_{t=t_{\text{NA}}} &= \mathcal{T}[E_{\text{in}}(t, \infty); t_0]_{t=t_{\text{NA}}} \\ &\quad + \varepsilon E_{\text{in}}(t_{\text{NA}}, \infty) \mathcal{T}[F(t - t_{\text{NA}}, \delta v_B); t_0]_{t=t_{\text{NA}}} \\ &= \sum_{n=0} b_n [t_{\text{NA}} - t_0]^n + \varepsilon E_{\text{in}}(t_{\text{NA}}, \infty) \left\{ \sum_{n=0} c_n [t_{\text{NA}} - t_0]^n \right\},\end{aligned}\quad (8)$$

where we may roughly estimate the magnitudes of the derivatives from the temporal durations of the functions as

$$b_n = \frac{d^n}{dt^n} E_{\text{in}}(t, \infty) \Big|_{t_0} \sim \left(\frac{1}{t_p} \right)^n, \quad (9a)$$

$$c_n = \frac{d^n}{dt^n} F(t - t_{\text{NA}}, \delta v_B) \Big|_{t_0} \sim F(t_{\text{NA}} - t_0, \delta v_B) (\delta v_B)^n. \quad (9b)$$

The prefactor $F(t_{\text{NA}} - t_0, \delta v_B)$ in Eq. (9b) represents the fact that the effect of the nonanalytical point weakens rapidly as $t_{\text{NA}} - t_0$ increases. The simplified analytical discussion based on Eq. (5) shows good agreement with the three cases numerically, shown in Figs. 8(b)–8(e).

For case I, we first consider that the bandwidth δv_B is very broad, as $\delta v_B \gg |t_{\text{NA}} - t_0|^{-1}$. In this case as $F(t_{\text{NA}} - t_0, \delta v_B) \ll 1$, then, $b_n \gg c_n$ in Eq. (9b). The term b_n is dominant in all regions of n considered. In this case, the expansion around t_0 develops beyond t_{NA} , predicting the Gaussian-shaped pulse, in good agreement with Fig. 8(b) ($\delta v_B = 50$ MHz).

Next, we consider case II in which the bandwidth is moderate, $\delta v_B > |t_{\text{NA}} - t_0|^{-1}$. In this case as $F(t, \delta v_B) < 1$, then, in the small- n regions, $b_n > c_n$, so b_n is dominant. With an increase in n , however, c_n terms become dominant, because the derivative series in the c_n terms in Eq. (9b) decreases more gently than in the b_n terms in Eq. (9a) as $t_p^{-1} < \delta v_B$. The critical order, $n_{\text{cri}}(\delta v_B)$ is understood as the order that satisfies

the condition $b_n \sim \varepsilon c_n$,

$$n_{\text{cri}}(\delta v_B) \sim \frac{\ln[\varepsilon F(t_{\text{NA}} - t_0, \delta v_B)]}{\ln[(t_p \delta v_B)^{-1}]}.\quad (10)$$

When the expansion develops beyond $n_{\text{cri}}(\delta v_B)$, the function becomes unstable at t_{NA} and diverges, in good agreement with Fig. 8(c) ($\delta v_B = 33$ MHz).

Finally, for case III, when the bandwidth of the filter is narrow, $\delta v_B \sim |t_{\text{NA}} - t_0|^{-1}$, then $F(t_{\text{NA}} - t_0, \delta v_B) \sim 1$, so $b_n \leq c_n$. The c_n terms are dominant or comparable to the b_n terms in all regions of n . In this case, the expansion around t_0 develops beyond t_{NA} , correctly predicting the filtered pulse shape after t_{NA} , in good agreement with Figs. 8(d) and 8(e) ($\delta v_B = 8.3$ and 5.0 MHz).

Note that the values of δv_B that separate the cases I, II, and III depend on the precision of the calculations. In our calculations, shown in Figs. 8(a)–8(f), the maximum order of the expansion was set to $n_{\text{max}} = 90$. For example, if we set this value as $n_{\text{max}} = 40$, the bandwidth $\delta v_B = 33$ MHz still belongs to case II, as we see $n_{\text{cri}}(\delta v_B = 33 \text{ MHz}) = 56$ in Fig. 8(g), line 3; thus, $n_{\text{max}} < n_{\text{cri}}$. Strictly, so long as the bandwidth δv_B is not infinite, then time point t_{NA} is not mathematically nonanalytical. Therefore, it may be supposed that the total shape of the filtered function could be predictable from the time point t_0 . This idea is reminiscent of a discussion that, mathematically, the Gaussian pulse has tails extending infinitely far back in time, so that the tiniest leading edge of a smooth Gaussian pulse could determine the entire pulse shape. Physically, however, such an expansion is impossible because we must take into account the effects of fluctuations, noise at the leading edge.

Studies aiming to reconcile the superluminal group velocity with relativistic causality should include a quantum-mechanical model of the photon detector, which in turn must take into account quantum fluctuations. In our discussion, the predictability of the forthcoming practical nonanalytical points depends on the maximum degree of expansion order; i.e., if the expansion can develop to a significantly higher order beyond n_{cri} , it can be used to predict further practical nonanalytical points. The degree of the expansion depends on the noise in the detector or, more fundamentally, on quantum fluctuations.

The fact that the forthcoming pulse shape is predictable under a condition of $\delta v_B \sim |t_{\text{NA}} - t_0|^{-1}$ is fairly reasonable. Consider an anomalous resonance line with width δv_R and consider a situation that a pulse with bandwidth δv_B propagates through the resonance under the condition $\delta v_B < \delta v_R$. In this case, the entire pulse shape is advanced without significant distortion by a time of the order of $\tau \sim -\delta v_R^{-1}$. Such a time advancement occurs generally within the time range of the predictability discussed above, as $|\tau| \sim |\delta v_R^{-1}| < |\delta v_B^{-1}| \sim |t_0 - t_{\text{NA}}|$.

V. SUMMARY

We examined the propagation velocity of information encoded as a nonanalytical point, controlling the sharpness of the point. When the bandwidth was sufficiently wide, the point propagated with luminal velocity in good agreement with relativistic causality. As the bandwidth was reduced, the propagation velocity converged to the relevant group velocity.

This transition was, however, qualitatively different in the fast and slow systems. From the point of view of relativistic causality, the fast propagation of the practical nonanalytical point indicates that the expansion around an early time point can predict the forthcoming pulse shape. It was shown that when the bandwidth was restricted below the critical value, the expansion predicted the forthcoming pulse shape well. Finally, we note that the pulse front, in a practical sense, that would also be relevant to the finite-bandwidth effect could be treated in a similar manner to the present one, in which a

discontinuous nonanalytical point exists at a very early time in the leading part of the pulse. Such an analysis could give an answer to the question set out in the Introduction as to whether a front is truly localized at an infinitesimal time point.

ACKNOWLEDGMENT

This work was supported by Japan Society for the Promotion of Science KAKENHI Grant No. 26287091.

-
- [1] S. Chu and S. Wong, Linear Pulse Propagation in an Absorbing Medium, *Phys. Rev. Lett.* **48**, 738 (1982).
- [2] A. I. Talukder, Y. Amagishi, and M. Tomita, Superluminal to Subluminal Transition in the Pulse Propagation in a Resonantly Absorbing Medium, *Phys. Rev. Lett.* **86**, 3546 (2001).
- [3] A. M. Steinberg and R. Y. Chiao, Dispersionless highly superluminal propagation in a medium with a gain doublet, *Phys. Rev. A* **49**, 2071 (1994).
- [4] L. J. Wang, A. Kuzmich, and A. Dogariu, Gain-assisted superluminal light propagation, *Nature (London)* **406**, 277 (2000).
- [5] K. Totsuka, N. Kobayashi, and M. Tomita, Slow Light in Coupled-Resonator-Induced Transparency, *Phys. Rev. Lett.* **98**, 213904 (2007).
- [6] K. Totsuka and M. Tomita, Slow and fast light in a microsphere-optical fiber system, *J. Opt. Soc. Am. B* **23**, 2194 (2006).
- [7] G. Dolling, C. Enkrich, M. Wegener, C. M. Soukoulis, and S. Linden, Simultaneous negative phase and group velocity of light in a metamaterial, *Science* **312**, 892 (2006).
- [8] D. Ye, G. Zheng, J. Wang, Z. Wang, S. Qiao, J. Huangfu, and L. Ran, Negative group velocity in the absence of absorption resonance, *Sci. Rep.* **3**, 1628 (2013).
- [9] A. M. Steinberg, P. G. Kwiat, and R. Y. Chiao, Measurement of the Single-Photon Tunneling Time, *Phys. Rev. Lett.* **71**, 708 (1993).
- [10] P. W. Milonni, *Fast Light, Slow Light and Left-Handed Light* (Taylor & Francis, New York, 2004).
- [11] L. Zhang, L. Zhan, K. Qian, J. Liu, Q. Shen, X. Hu, and S. Luo, Superluminal Propagation at Negative Group Velocity in Optical Fibers Based on Brillouin Lasing Oscillation, *Phys. Rev. Lett.* **107**, 093903 (2011).
- [12] E. L. Bolda and R. Y. Chiao, Two theorems for the group velocity in dispersive media, *Phys. Rev. A* **48**, 3890 (1993).
- [13] G. Diener, Superluminal group velocities and information transfer, *Phys. Lett. A* **223**, 327 (1996).
- [14] J. C. Garrison, M. W. Mitchell, R. Y. Chiao, and E. L. Bolda, Superluminal signals: causal loop paradoxes revisited, *Phys. Lett. A* **245**, 19 (1998).
- [15] K. Wynne, Causality and the nature of information, *Opt. Commun.* **209**, 85 (2002).
- [16] B. Macke and B. Segard, Propagation of light-pulses at a negative group-velocity, *Eur. Phys. J. D* **23**, 125 (2003).
- [17] M. Tomita, H. Amano, S. Masegi, and A. I. Talukder, Direct Observation of a Pulse Peak Using a Peak-Removed Gaussian Optical Pulse in a Superluminal Medium, *Phys. Rev. Lett.* **112**, 093903 (2014).
- [18] L. Brillouin, *Wave Propagation and Group Velocity* (Academic Press, New York, 1960).
- [19] N. Brunner, V. Scarani, M. Wegmüller, M. Legré, and N. Gisin, Direct Measurement of Superluminal Group Velocity and Signal Velocity in an Optical Fiber, *Phys. Rev. Lett.* **93**, 203902 (2004).
- [20] D. Ye, Y. Salamin, J. Huangfu, S. Qiao, G. Zheng, and L. Ran, Observation of wave packet distortion during a negative-group-velocity transmission, *Sci. Rep.* **5**, 8100 (2015).
- [21] R. Y. Chiao and A. M. Steinberg, *Tunneling Times and Superluminality*, Vol. 37 of Progress in Optics, edited by E. Wolf (Elsevier, Amsterdam, 1997), p. 345.
- [22] M. D. Stenner, D. J. Gauthier, and M. A. Neifeld, The speed of information in a ‘fast-light’ optical medium, *Nature (London)* **425**, 695 (2003).
- [23] M. D. Stenner, D. J. Gauthier, and M. A. Neifeld, Fast Causal Information Transmission in a Medium With a Slow Group Velocity, *Phys. Rev. Lett.* **94**, 053902 (2005).
- [24] M. Tomita, H. Uesugi, P. Sultana, and T. Oishi, Causal information velocity in fast and slow pulse propagation in an optical ring resonator, *Phys. Rev. A* **84**, 043843 (2011).
- [25] A. Kuzmich, A. Dogariu, L. J. Wang, P. W. Milonni, and R. Y. Chiao, Signal Velocity, Causality, and Quantum Noise in Superluminal Light Pulse Propagation, *Phys. Rev. Lett.* **86**, 3925 (2001).
- [26] U. Vogl, R. T. Glasser, and P. D. Lett, Advanced detection of information in optical pulses with negative group velocity, *Phys. Rev. A* **86**, 031806(R) (2012).
- [27] A. H. Dorrah and M. Mojahedi, Velocity of detectable information in faster-than-light pulses, *Phys. Rev. A* **90**, 033822 (2014).
- [28] Z. Yang, Physical mechanism and information velocity of fast light: A time-domain analysis, *Phys. Rev. A* **87**, 023801 (2013).
- [29] H. Amano and M. Tomita, Luminal pulse velocity in a superluminal medium, *Phys. Rev. A* **92**, 063837 (2015).
- [30] R. Suzuki and M. Tomita, Causal propagation of nonanalytical points in fast- and slow-light media, *Phys. Rev. A* **88**, 053822 (2013).